ACS Photonics

Letter

pubs.acs.org/journal/apchd5

All-Optical Modulation of a Graphene-Cladded Silicon Photonic Crystal Cavity

Zhe Shi,[†] Lin Gan,*[,†] Ting-Hui Xiao, Hong-Lian Guo, and Zhi-Yuan Li*

Laboratory of Optical Physics, Institute of Physics, Chinese Academy of Sciences, P.O. Box 603, Beijing 100190, China

Supporting Information

ABSTRACT: The combination of graphene and a silicon photonic crystal cavity provides an ideal structure for realizing sensitive all-optical modulation. In this paper, an all-optical tuning of a graphene-cladded photonic crystal cavity is demonstrated. A 3.5 nm resonance wavelength shift and a 20% quality factor change are observed as a 1064 nm continuous-wave control laser is focused on the cavity. The resonance wavelength shift is nearly 2 times that realized with electrical modulation and can be further improved with increasing laser power. Meanwhile, it is found that the laser power to reach the saturation absorption state of graphene is nearly 2 orders of magnitude lower than that for monolayer graphene on silica. The experimental results are attributed to optically induced transparency and hot carrier effects. This study opens up a promising way to construct a sensitive all-optical modulator, which is a necessary device in an all-optical integrated circuit, by using a graphene-cladded photonic crystal cavity.

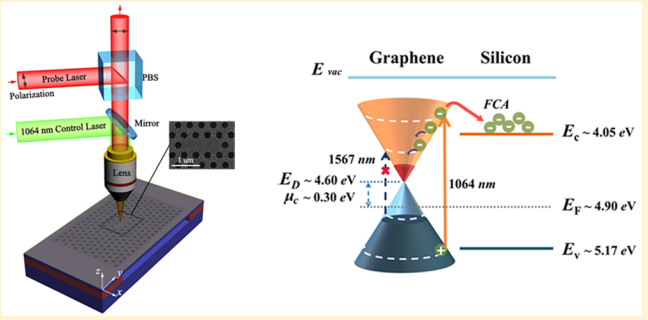

KEYWORDS: *all-optical modulation, graphene, optically induced transparency, photonic crystal cavity*

All-optical integrated circuits have attracted extensive interest due to their benefits in broad bandwidth, high information capacity, low loss, and so on.[1] Several basic silicon structures, such as coupler, cavity, filter, and switch,[2−5] have been made in a silicon-on-insulator (SOI) platform for photonic integrated circuits. Besides, silicon photonic crystal (PhC) structures,[6] especially PhC microcavities,[7] have been demonstrated possessing many important functions due to their small mode volume and high quality (Q) factor. The externally dynamical tuning of the operating wavelength of a cavity is one of the key issues to match distinct practical applications. Various tuning techniques, such as optical pumping,[4] thermal tuning,[8] atomic layer deposition,[9] and local oxidation,[10] have been demonstrated to solve this important problem. Very recently, an active way of electrical control of a PhC cavity by graphene was reported,[11−14] where graphene plays an important role of an absorber and a 2 nm resonant wavelength shift was observed. Several tunable integrated graphene−silicon modulators,[15] detectors,[16−18] and couplers[19] were also reported. As is well known, graphene, a single layer of carbon atoms in a honeycomb lattice with linear electronic energy dispersion,[20] has attracted significant attention due to its unique optoelectronic properties.[21,22] Although suspended monolayer graphene has a constant absorption coefficient of about 2.3% over a wide spectral range, this absorption can be modulated by external light owing to the optically induced transparency (OIT) effect.[23−25] However, up to now, there are few all-optical modulations based on graphene[25,26] reported, and all of them are studied based on a waveguide system coated with graphene. In a recent work,[25] Yu et al. reported a less than 1 dB signal change in a waveguide system with a size of several hundred micrometers under a high photon energy light pumping, where the pumping light can be absorbed by both graphene and a silicon waveguide. They ascribed the optical modulation to the optical OIT of graphene due to heat carrier relaxation in graphene and photoinduced carrier transfer from the silicon layer to graphene. To achieve high optical modulation and improve optical integration, an all-optical modulation with a graphene-coated PhC cavity could be a better choice, because a PhC cavity has a small mode volume and high Q factor, which are important for light confinement and allow for large optical modulation.

In this work, an all-optical modulation of a graphene-cladded PhC cavity is demonstrated for the first time, which enables realizing a 3.5 nm resonance wavelength shift and a near 20% change in the Q factor when a 1064 nm continuous-wave (CW) control laser is illuminated on the cavity. The photon energy of 1064 nm light is less than the band gap of silicon, so it can only be absorbed by graphene, which is different from the case in ref 25, where illuminated light can be absorbed by both graphene and the silicon waveguide. Furthermore, the mechanism governing the optical modulation in our case is slightly different from that reported in ref 25, where they ascribed the optical modulation to the OIT effect. But in our case, the

Received: May 11, 2015
Published: October 29, 2015

ACS Publications © 2015 American Chemical Society

DOI: 10.1021/acsphotonics.5b00469
ACS Photonics 2015, 2, 1513−1518

OIT effect and free carrier absorption (FCA) as well as free carrier dispersion (FCD) effect play inseparable roles in realizing optical modulation of our hybrid structure of graphene on a PhC cavity. Comparing with the modulation effect of graphene on a waveguide structure, a 20% Q factor change is much more prominent with an only 1.5 μm interaction scale, which suggests much stronger interaction existing in graphene on a PhC cavity. In addition, our all-optical modulation devices are much easier to fabricate compared with that of electrical modulation. All of the above indicate that this hybrid graphene PhC cavity structure could be potentially very useful for constructing all-optical switching and modulating devices.

EXPERIMENTAL RESULTS

A cross-polarized reflectivity measurement on the hybrid structure of graphene covered on the PhC cavity is adopted[27] as schematically shown in Figure 1, where the hybrid structure

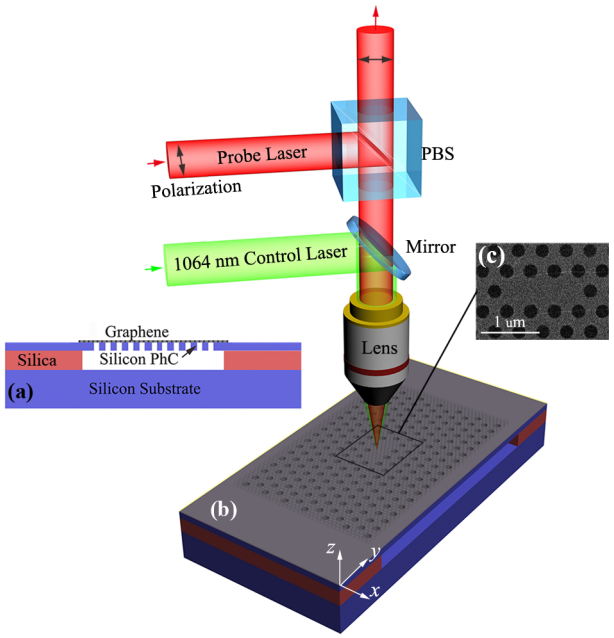

Figure 1. Experimental setup. (a) Schematic cross section of a graphene-cladded silicon PhC cavity structure built in a silicon layer with a thickness of 220 nm and lattice constant of 420 nm. (b) Schematic of a cross-polarized reflectivity measurement system. The probe light is a narrow-band tunable semiconductor laser around 1550 nm, and the control laser is a 1064 nm laser. (c) SEM image of the graphene-cladded silicon PhC cavity.

and its scanning electron microscopy (SEM) image are also shown in Figure 1a and c. A tunable infrared laser at a center wavelength of 1550 nm is used as the probe light, and a CW laser of 1064 nm focused on the cavity with a beam spot of about 5 μm is used as a control light, both of which are schematically shown in Figure 1b. In our experiments, the control laser intensity is changed and the reflection spectrum of the probe laser on the hybrid graphene−PhC cavity is collected. In Figure 1c, it is noticed that graphene is smoothly laid on the PhC without any discernible inhomogeneity, and its Raman spectrum as shown in Figure 2a indicates that the graphene is monolayer[28] and high quality (a detailed analysis is in section 1 of the Supporting Information). In reference to Das's experimental results,[29] it is inferred that the graphene on our cavity is p-type doped with a Fermi energy E_F of about 0.3−

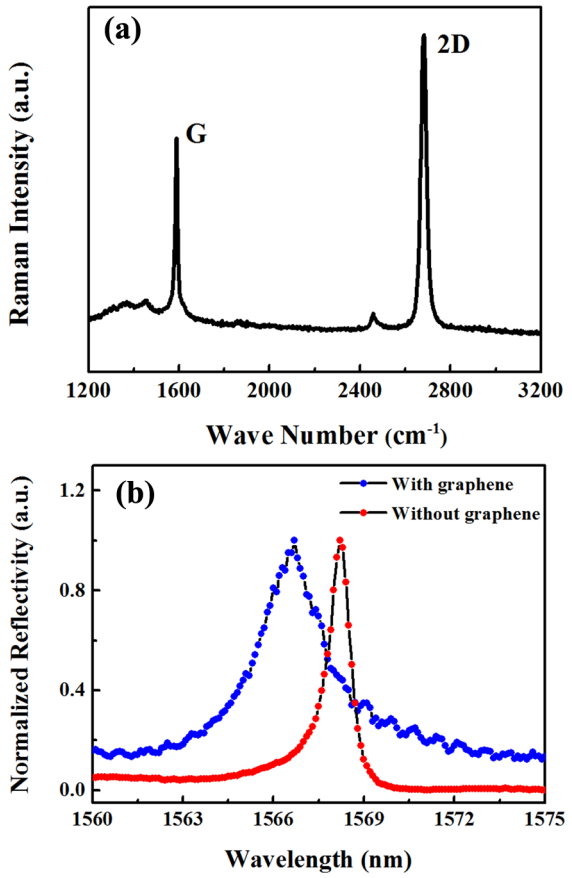

Figure 2. Raman spectrum of graphene and reflectivity of the hybrid PhC. (a) Raman spectrum of a transferred graphene on top of the silicon cavity. (b) Reflectivity spectrum of PhC L3 cavities without (red line) and with (blue line) graphene.

0.35 eV below the Dirac point, consistent with the estimated results of ref 30. Figure 2b shows the normalized reflectivity spectrum of PhC L3 cavities with and without the graphene layer. The absorption of graphene causes a broadening of the resonance peak and a Q factor decreasing from 1909 to 594. Similar phenomena are observed by other groups as reported in recent experiments.[11−13]

The effect of control light on the hybrid structure of graphene on PhC is systematically investigated. The control light is weakly absorbed by the silicon substrate because of a very small absorption coefficient, α = 11.1 cm^{-1}, for the 1064 nm light.[31] Figure 3a shows the normalized reflection spectra expressed by the solid curves at several control laser powers. The dotted curves are fitted by Lorentzian profiles. An obvious red-shift in resonance wavelength and a broadening of the resonance peak are clearly observed with the increase of pumping power. The Q factor and resonance peak wavelength changes with the control laser power ranging from 0 to 50 mW are shown in Figure 3b and c, respectively. The Q factor, as presented with the square symbols in Figure 3b, first drops from 600 to 480, then rises to 560. In Figure 3c, a near linear relation between the control laser power and the resonance wavelength is found. For comparison, the Q factor and the resonance wavelength of the same cavity after turning off the control laser are measured, and the results are shown in Figure 3b and c with the circle symbols. The same Q factor and the resonance wavelength at zero control laser power before and after the control laser is applied clearly indicate that the

DOI: 10.1021/acsphotonics.5b00469
ACS Photonics 2015, 2, 1513−1518

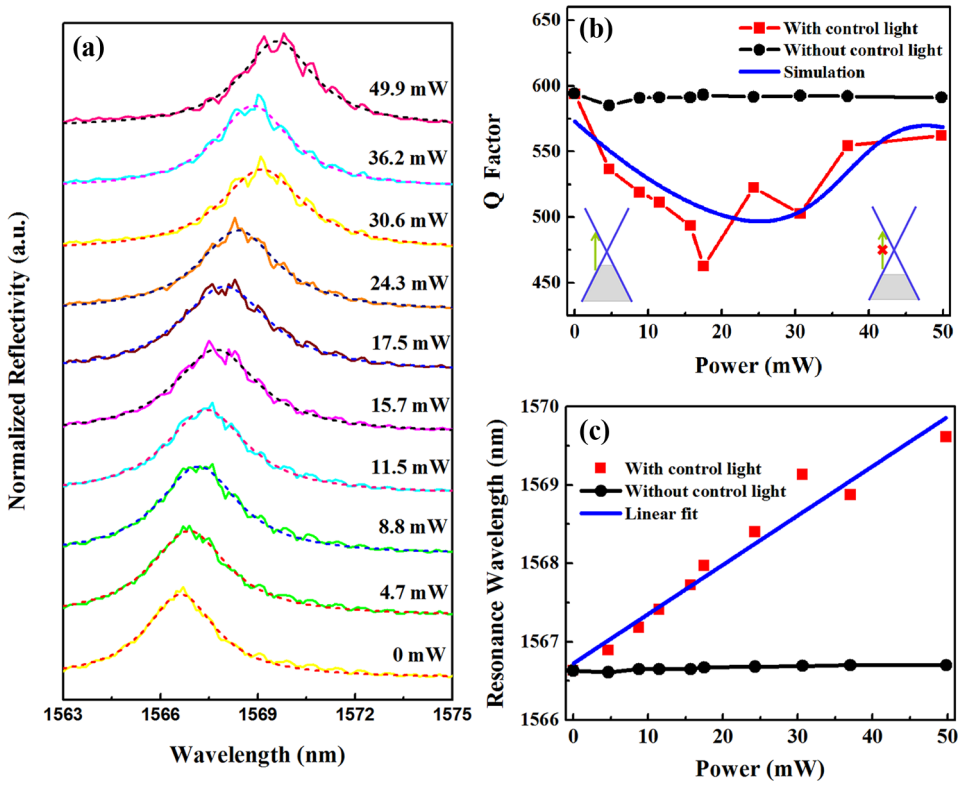

Figure 3. Measured optical properties of the hybrid graphene−PhC cavity. (a) Normalized reflectivity spectra of the graphene-cladded PhC cavity. The dashed lines are Lorentzian fitting to the experimental data. (b) Cavity Q factor changes with control laser powers. The inset on the left (right) is a schematic energy band diagram of the graphene at an absorbable (saturation) state to the probe light. (c) Resonance wavelength variation with control laser powers. The disperse symbols are experimental data with (squares)/without (circles) the control light.

graphene-cladded PhC cavity is not damaged by the control laser even when such a high power as 50 mW is applied. In order to prove that the cavity modulation is induced by graphene, a control experiment on the cavity without graphene is also done under the same conditions. The experimental results show that the resonant wavelength shift without graphene is 1.9 pm/mW, which is much smaller (34 times smaller) than the value of 61.9 pm/mW with graphene. The line width variation is less than 0.02 nm without graphene, much smaller than the value of 0.74 nm with graphene. The experiment data and analysis are given in section 3 of the Supporting Information. Therefore, the observed phenomena here can be dominantly ascribed to the contribution of graphene.

■ ANALYSIS AND DISCUSSION

A theoretical explanation of the change of the cavity resonance wavelength and Q factor induced by the control laser is highly interesting and critically important for better understanding of the optoelectronic physics involved in the graphene-cladded PhC cavity. A schematic energy band diagram of the graphene/silicon heterostructure is plotted in Figure 4 to help understand the origins of the observed phenomena. The silicon wafer is p-type doped with a boron concentration of about 10^{15} cm^{-3}, as confirmed by secondary ion mass spectrometry (SIMS) measurement. The corresponding Fermi level is about −4.9 eV relative to the vacuum level.[32] In comparison, as mentioned above, the Fermi level, μ_c, of graphene is about 0.3 eV below the Dirac point, which is located at about −4.60 eV relative to the vacuum level.[33] That means the Fermi level of graphene is about −4.9 eV relative to the vacuum level. The similar Fermi

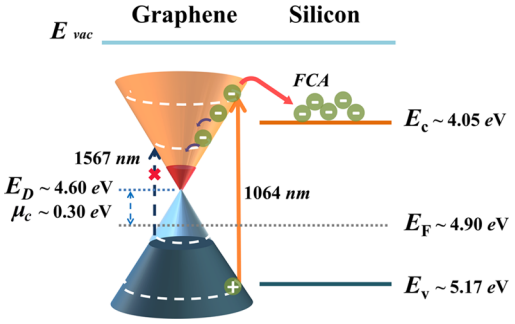

Figure 4. Optoelectronic processes in our all-optical modulation. E_C, E_V, and E_F are the conduction, valence bands, and Fermi level of silicon, respectively; E_D is the Dirac point, and μ_c is the Fermi level of graphene. A 1064 nm control laser excites carriers in graphene, and some of them transfer to the silicon layer, resulting in lowering of the graphene Fermi level and blocking further absorption of graphene to the probe light.

levels of graphene and silicon indicated that energy band bending of silicon at the interface between graphene and silicon is ignorable. For the 1064 nm (1.16 eV) control laser, the photon energy is much greater than twice the Fermi level ($2|\mu_c|$) of graphene. Thus, the control laser can excite electrons in graphene transiting from the valence band to the conduction band. Meanwhile, the absorption of silicon to control light can be ignored due to its small absorption coefficient (a discussion on linear and nonlinear absorption of silicon is given in section 4 of the Supporting Information). However, for a probe laser around 1550 nm (0.8 eV), its photon energy is only slightly larger than $2|\mu_c|$ of graphene, but is far smaller than that of the

DOI: 10.1021/acsphotonics.5b00469
ACS Photonics 2015, 2, 1513−1518

control light. With the control laser on, electrons in graphene are excited from the valence band to the conduction band and partly transfer to silicon,[26] and this causes the unoccupied state in the valence band of graphene to go down gradually. As the control laser power increases to a critical power level, the absorption of electrons in graphene upon the probe laser is blocked and then graphene reaches the saturation absorption state. During the process, the Q factor first decreases gradually with the control laser power and then begins to increase at the critical power, which is about 25 mW here, as shown in Figure 3b. In this case, the silicon substrate helps to achieve the OIT state, in which graphene becomes transparent to the probe light.

In the experiment, the intrinsic Q factor of the cavity without graphene is $Q_0 = 1909$. The Q factor change due to the absorption of graphene and free carriers in silicon to the probe light can be described as $(1/Q) = (1/Q_0) + (1/Q_{ABS}) + (1/Q_{FCA})$. Here Q_{ABS} is an equivalent contribution of graphene absorbing probe light to the Q factor, $(1/Q_{ABS}) = (\sigma_g/\varepsilon_0\varepsilon_r\omega_0 d)\exp(-(nd/\lambda))$ (a detailed derivation of graphene optical conductivity is given in section 6 of the Supporting Information), and Q_{FCA} denotes the contribution of FCA to the Q factor. In Q_{ABS}, σ_g is the optical conductivity of graphene, ε_0 is the vacuum permittivity, ε_r is the dielectric constant of graphene, ω_0 and λ are the frequency and wavelength of the cavity resonance peak, and n and d are the refractive index and the thickness of silicon. According to a theory of rate equation and a supposition that each photon generates a free electron−hole pair, the photogenerated carrier concentration in graphene can be simply deduced from the relation with the power density P of the control light, $N_0 = (\alpha_c P/\hbar\omega)\tau_{tr}$,[26] where $\alpha_c = 1.132\%$ is an effective absorption coefficient of graphene on PhC (see section 5 of the Supporting Information), $\tau_{tr} = 1\ \mu s$ is the nonequilibrium carrier recombination time deduced from a transient process of cavity reflection intensity under a 1064 nm control laser (see the details in section 7 of the Supporting Information), and ω is the frequency of the control laser. Here we have neglected the radiation recombination when taking into account the power level of the control laser.[34] When the control light is on, some of the photoinduced carriers are transferred from graphene to the silicon PhC, which results in FCA to the probe light in silicon. The Q_{FCA} factor due to FCA in silicon can be described as $Q_{FCA} = (2\pi n/\alpha_{FCA}\lambda)$,[35] where α_{FCA} is the FCA coefficient of silicon at 1550 nm described by $\alpha_{FCA} = 1.45 \times 10^{-17} N\ (cm^{-1})$, where N is the free carrier concentration of silicon in unit of cm^{-3}. It can be seen that Q_{FCA} is inversely proportional to the free carrier concentration of silicon.

When carriers transfer from graphene to silicon, an electric field is built by electrons accumulated in silicon and reduces the further transfer of electrons from graphene to silicon. For simplicity, we just consider an average transfer efficiency T of electron from graphene to silicon. The average carrier area density is $Nd = TN_0$ in the area illuminated by the 1064 nm control laser, where $d = 220$ nm is the thickness of silicon. By simulation of our experimental Q curve based on the Q model, the carrier numbers are obtained to be about $9 \times 10^{18}\ cm^{-3}$ under a 50 mW 1064 nm laser. This indicates that the carrier transfer efficiency is about 1.1%. Based on the above analysis, a simulation of the Q factor versus the power of the control laser is made, and the result is shown by the blue line in Figure 3b. A good agreement with the experimental results is obtained. When the power of the control laser is lower than the critical power of 25 mW, the graphene layer does not reach saturation absorption for the 1550 nm probe laser and the Q_{ABS} factor related to the absorption of graphene increases slightly. At the same time, the Q_{FCA} factor decreases quickly, and this causes the total Q factor to decrease to 480. After that, as the control laser power exceeds 25 mW, which corresponds to a pump power density of about 0.01 MW/cm^2, the graphene layer reaches a saturation absorption state and becomes more and more transparent to the probe light. The observed saturation absorption power density of 0.01 MW/cm^2 here is nearly 2 orders of magnitude lower than that reported in ref 19. The lower saturation absorption power in graphene on silicon is mainly due to the excited electron in graphene transferred to silicon, which results in a dynamic decrease of the Fermi level of graphene compared with the case of graphene on silica. During this process, Q_{ABS} increases more quickly than the decrease of Q_{FCA}, leading to an increase of the total Q factor from 480 to 560. It clearly turns out that the Q factor of our hybrid graphene−PhC cavity device is a consequence of the complicated competition of saturation absorption in graphene and FCA in silicon under different control laser powers.

We adopt the above physical picture to further examine the shift of resonance wavelength. As shown in Figure 3c, the resonance wavelength increases with the control laser power at a rate of 61.9 pm/mW. This red-shift is predominated by the thermo-optic effect due to FCA on the refractive index of silicon, although both FCA and FCD play roles here. Since the hole concentration variation is ignorable in silicon, its contribution to the change of n is not necessary to consider. So only the electron concentration change is considered here. The refractive index change of silicon with its carrier concentration has a relation $\Delta n = -8.8 \times 10^{-22} N$.[35] According to the above simulation result, the maximum carrier concentration N can reach a high value of $9 \times 10^{18}\ cm^{-3}$. Correspondingly, the refractive index change induced by FCD is −0.008. For the FCA effect, the transferred carriers from graphene to silicon absorb light energy, resulting in a rise in temperature. The change of the refractive index of silicon with temperature is $(dn/dT) = 1.86 \times 10^{-4}\ K^{-1}$ at 1550 nm.[36] According to our experimental and simulation results, the FCA effect induced refractive index change can reach a value of +0.015, corresponding to a temperature increase of about 80 K. So a net effect of FCA and FCD results in an increase of refractive index, and a 3.4 nm resonant wavelength shift is observed in our experiments. Therefore, the competition between the relatively stronger thermal-optic effect due to FCA in silicon and the relatively weaker FCD in silicon leads to the red-shift in the resonance wavelength of the hybrid graphene−PhC cavity with respect to the control laser power.

CONCLUSIONS

In conclusion, an all-optical tuning of a graphene-cladded silicon PhC cavity has been demonstrated for the first time experimentally. Several unique properties such as large resonance wavelength shift, Q factor change, and about 2 orders of magnitude lower saturation absorption than that for monolayer graphene on silica have been found. The resonance wavelength shift is near 2 times that realized with electrical modulation and can be further improved with increasing the pump laser power. A quantitative simulation on the Q factor change with control laser power agrees well with the experimental result. All of the results can be ascribed to the OIT, FCA, and FCD effects in this hybrid structure, which

DOI: 10.1021/acsphotonics.5b00469
ACS Photonics 2015, 2, 1513−1518

involves complicated optoelectronic physical processes. These experimental and theoretical results indicate that the hybrid structure of graphene on PhC not only is a valuable platform for studying all-optical modulation processes and mechanisms but also has promising potential applications in all optical devices such as sensitive optical switches and optical tuning devices.

METHODS

Fabrication. The PhC cavity is fabricated on an SOI wafer (SOITEC) with a 220 nm thick top silicon layer on a 3 μm thick cladding silica layer. Electron-beam lithography (EBL) and inductively coupled plasma (ICP) techniques are used to make a PhC cavity in a hexagonal lattice with a lattice constant of 420 nm and a radius of air holes of 115 nm. Then the wafer is etched by buffered hydrofluoric acid to remove the cladding silica layer. A large-area monolayer of graphene grown by CVD was transferred to our PhC to form the hybrid graphene−PhC cavity structure.[37] The transferred graphene on the PhC L3 cavity is characterized by SEM and Raman spectroscopy (see details in the Supporting Information).

Cross-Polarized Reflectivity Measurement. The hybrid graphene−PhC cavity structure is horizontally placed in the *XOY* plane, and the long axis of the cavity is along the *x*-axis direction. A tunable laser source (Agilent 8163B) with wavelength tuning from 1520 to 1630 nm is used as the probe light. It is linearly polarized, and its polarization direction is at 45° angle relative to the cavity axis. The probe light is reflected and scattered by the hybrid structure. The cavity-radiated signal is detected, which might be polarized in all directions. A polarized beam splitter is used to block those strong background signals coming from mirror reflection of the incident probe light by the silicon PhC and only allows the signals in the orthogonal polarized direction (at the −45° direction) to pass. Eventually the signal is probed and analyzed by a power meter.

ASSOCIATED CONTENT

Supporting Information

The Supporting Information is available free of charge on the ACS Publications website at DOI: 10.1021/acsphotonics.5b00469.

Raman spectroscopy of graphene, SIMS measurement of silicon, control experiment on a silicon photonic crystal cavity without graphene, optical conductivity of graphene, effective absorption coefficient of graphene on PhC, transient state process of a cavity reflection, detailed theoretical calculation of the *Q* factor of graphene-cladded silicon cavity, and estimate of resonance wavelength with refractive index of silicon (PDF)

AUTHOR INFORMATION

Corresponding Authors

*E-mail: lgan@aphy.iphy.ac.cn.
*E-mail: lizy@aphy.iphy.ac.cn.

Author Contributions

†Zhe Shi and Lin Gan contributed equally.

Notes

The authors declare no competing financial interest.

ACKNOWLEDGMENTS

The authors would like to thank Hao Wang for help with the growth of graphene, Chengchun Tang for help with the EBL technique, and Prof. Arka Majumdar for discussion on cross-polarized reflectivity measurement of the graphene/silicon structure. This work is supported by the National Natural Science Foundation of China (Nos. 11204365 and 11434017) and 973 Program of China (No. 2013CB632704).

REFERENCES

(1) Li, Z. Y. Optics and photonics at nanoscale: Principles and perspectives. *EPL (Europhysics Letters)* **2015**, *110*, 14001.
(2) Taillaert, D.; Bienstman, P.; Baets, R. Compact efficient broadband grating coupler for silicon-on-insulator waveguides. *Opt. Lett.* **2004**, *29*, 2749−2751.
(3) Vahala, K. J. Optical microcavities. *Nature* **2003**, *424*, 839−846.
(4) Li, Z. Y.; Meng, Z. M. Polystyrene Kerr nonlinear photonic crystals for building ultrafast optical switching and logic devices. *J. Mater. Chem. C* **2014**, *2*, 783−800.
(5) Koos, C.; Vorreau, P.; Vallaitis, V.; Dumon, P.; Bogaerts, W.; Baets, R.; Esembeson, B.; Biaggio, I.; Michinobu, T.; Diederich, F.; Freude, W.; Leuthold, J. All-optical high-speed signal processing with silicon-organic hybrid slot waveguides. *Nat. Photonics* **2009**, *3*, 216−219.
(6) Mekis, A.; Chen, J. C.; Kurland, I.; Fan, S. H.; Villeneuve, P. R.; Joannopoulos, J. D. High transmission through sharp bends in photonic crystal waveguides. *Phys. Rev. Lett.* **1996**, *77*, 3787−3790.
(7) Akahane, Y.; Asano, T.; Song, B. S.; Noda, S. High-Q photonic nanocavity in a two-dimensional photonic crystal. *Nature* **2003**, *425*, 944−947.
(8) Faraon, A.; Englund, D.; Fushman, I.; Vuckovic, J.; Stoltz, N.; Petroff, P. Local quantum dot tuning on photonic crystal chips. *Appl. Phys. Lett.* **2007**, *90*, 213110.
(9) Yang, X. D.; Chen, C. J.; Husko, C. A.; Wong, C. W. Digital resonance tuning of high-Q/V_m silicon photonic crystal nanocavities by atomic layer deposition. *Appl. Phys. Lett.* **2007**, *91*, 161114.
(10) Hennessy, K.; Hogerle, C.; Hu, E.; Badolato, A.; Imamogulu, A. Tuning photonic nanocavities by atomic force microscope nano-oxidation. *Appl. Phys. Lett.* **2006**, *89*, 041118.
(11) Majumdar, A.; Kim, J.; Vuckovic, J.; Wang, F. Electrical control of silicon photonic crystal cavity by graphene. *Nano Lett.* **2013**, *13*, 515−518.
(12) Gan, X. T.; Mak, K. F.; Gao, Y. D.; You, Y. M.; Hatami, F.; Hone, J.; Heinz, T. F.; Englund, D. Strong enhancement of light-matter interaction in graphene coupled to a photonic crystal nanocavity. *Nano Lett.* **2012**, *12*, 5626−5631.
(13) Gan, X. T.; Shiue, R. J.; Gao, Y. D.; Mak, K. F.; Yao, X. W.; Li, L. Z.; Szep, A.; Walker, D.; Hone, J.; Heinz, T. F.; Englund, D. High-Contrast Electrooptic Modulation of a Photonic Crystal Nanocavity by Electrical Gating of Graphene. *Nano Lett.* **2013**, *13*, 691−696.
(14) Gu, T.; Petrone, N.; McMillan, J. F.; van der Zande, A.; Yu, M.; Lo, G. Q.; Kwong, D. L.; Hone, J.; Wong, C. W. Regenerative oscillation and four-wave mixing in graphene optoelectronics. *Nat. Photonics* **2012**, *6*, 554−559.
(15) Liu, M.; Yin, X. B.; Ulin-Avila, E.; Geng, B. S.; Zentgraf, T.; Ju, L.; Wang, F.; Zhang, X. A graphene-based broadband optical modulator. *Nature* **2011**, *474*, 64−67.
(16) Xia, F. N.; Mueller, T.; Lin, Y. M.; Valdes-Garcia, A.; Avouris, P. Ultrafast graphene photodetector. *Nat. Nanotechnol.* **2009**, *4*, 839−843.
(17) Mueller, T.; Xia, F. N.; Avouris, P. Graphene photodetectors for high-speed optical communications. *Nat. Photonics* **2010**, *4*, 297−301.
(18) Koppens, F. H. L.; Mueller, T.; Avouris, P.; Ferrari, A. C.; Vitiello, M. S.; Polini, M. Photodetectors based on graphene, other two-dimensional materials and hybrid systems. *Nat. Nanotechnol.* **2014**, *9*, 780−793.

DOI: 10.1021/acsphotonics.5b00469
ACS Photonics 2015, 2, 1513−1518

(19) Cheng, Z. Z.; Li, Z.; Xu, K.; Tsang, H. K. Increase of the grating coupler bandwidth with a graphene overlay. *Appl. Phys. Lett.* **2014**, *104*, 111109.
(20) Geim, A. K.; Novoselov, K. S. The rise of graphene. *Nat. Mater.* **2007**, *6*, 183−191.
(21) Bonaccorso, F.; Sun, Z.; Hasan, T.; Ferrari, A. C. Graphene photonics and optoelectronics. *Nat. Photonics* **2010**, *4*, 611−622.
(22) Bao, Q. L.; Loh, K. P. Graphene photonics, plasmonics, and broadband optoelectronic devices. *ACS Nano* **2012**, *6*, 3677−3694.
(23) Bao, Q. L.; Zhang, H.; Wang, Y.; Ni, Z. H.; Yan, Y. L.; Shen, Z. X.; Loh, K. P.; Tang, D. Y. Atomic-layer graphene as a saturable absorber for ultrafast pulsed lasers. *Adv. Funct. Mater.* **2009**, *19*, 3077−3083.
(24) Li, W.; Chen, B.; Meng, C.; Fang, W.; Xiao, Y.; Li, X. Y.; Hu, Z. F.; Xu, Y. X.; Tong, L. M.; Wang, H. Q.; et al. Ultrafast all-optical graphene modulator. *Nano Lett.* **2014**, *14*, 955−959.
(25) Yu, L. H.; Zheng, J. J.; Xu, Y.; Dai, D. X.; He, S. L. Local and non local optically induced transparency effects in graphene-silicon hybrid nanophotonic integrated circuits. *ACS Nano* **2014**, *8*, 11386−11393.
(26) Cheng, Z. Z.; Tsang, H. K.; Wang, X. M.; Xu, K.; Xu, J. B. In-Plane Optical absorption and free carrier absorption in graphene-on-silicon waveguides. *IEEE J. Sel. Top. Quantum Electron.* **2014**, *20*, 4400106.
(27) Englund, D.; Faraon, A.; Fushman, I.; Stoltz, N.; Petroff, P.; Vuckovic, J. Controlling cavity reflectivity with a single quantum dot. *Nature* **2007**, *450*, 857−861.
(28) Ferrari, A. C.; Meyer, J. C.; Scardaci, V.; Casiraghi, C.; Lazzeri, M.; Piscanec, S.; Jiang, D.; Novoselov, K. S.; Roth, S.; Geim, A. K. Raman spectrum of graphene and graphene layers. *Phys. Rev. Lett.* **2006**, *97*, 187401.
(29) Das, A.; Pisana, S.; Chakraborty, B.; Piscanec, S.; Saha, S. K.; Waghmare, U. V.; Novoselov, K. S.; Krishnamurthy, H. R.; Geim, A. K.; Ferrari, A. C.; Sood, A. K. Monitoring dopants by Raman scattering in an electrochemically top-gated graphene transistor. *Nat. Nanotechnol.* **2008**, *3*, 210−215.
(30) Wang, X. M.; Cheng, Z. Z.; Xu, K.; Tsang, H. K.; Xu, J. B. High-responsivity graphene/silicon-heterostructure waveguide photodetectors. *Nat. Photonics* **2013**, *7*, 888−891.
(31) Green, M. A.; Keevers, M. J. Optical Properties of Intrinsic Silicon at 300 K. *Prog. Photovoltaics* **1995**, *3*, 189−192.
(32) Sze, S. M.; Ng, K. K. *Physics of Semiconductor Devices*, 3rd ed.; John Wiley & Sons: Hoboken, NJ, 2007.
(33) Yu, Y.; Zhao, Y.; Ryu, S.; Brus, L. E.; Kim, K. S.; et al. Tuning the graphene work function by electric field effect. *Nano Lett.* **2009**, *9*, 3430−3434.
(34) Reed, G. T.; Mashanovich, G.; Gardes, F. Y.; Thomson, D. J. Silicon optical modulators. *Nat. Photonics* **2010**, *4*, 518−526.
(35) EI Kurdi, M.; Checoury, X.; David, S.; Ngo, T. P.; Zerounian, N.; et al. Quality factor of Si-based photonic crystal L3 nanocavities probed with an internal source. *Opt. Express* **2008**, *16*, 8780−8791.
(36) Horvath, C.; Bachman, D.; Indoe, R.; Van, V. Photothermal nonlinearity and optical bistability in a graphene-silicon waveguide resonator. *Opt. Lett.* **2013**, *38*, 5036−5039.
(37) Li, X. S.; Zhu, Y. W.; Cai, W. W.; Borysiak, M.; Han, B. Y.; Chen, D.; Piner, R. D.; Colombo, L.; Ruoff, R. S. Transfer of large-area graphene films for high-performance transparent conductive electrodes. *Nano Lett.* **2009**, *9*, 4359−4363.

DOI: 10.1021/acsphotonics.5b00469
ACS Photonics 2015, 2, 1513−1518